## SUPPLEMENTARY METHODS

### Magnetic resonance imaging

Magnetic resonance imaging was performed on transgenic mice as described previously [1]. Lung tumor burden was monitored by MR imaging monthly until the emergence of resistant tumors, then more frequently thereafter. When mice with osimertinib-resistant tumors were switched to another TKI, they were scanned 1-2 times per week to monitor response. Tumor volume was quantified by calculating the area of visible lung opacities present in each image sequence per mouse using BioImage Suite 3.01 [2].

### *In vivo* TKI Treatments

Osimertinib (AstraZeneca), erlotinib and afatinib (Organic Synthesis Core Facility at MSKCC, NY) were resuspended in 0.5% methylcellulose. Mice were treated with 5 mg/kg or 25 mg/kg TKI daily Monday-Friday once they had been on dox for ~6 weeks and developed tumors. Osimertinib and afatinib were given orally, and erlotinib was given intraperitoneally. The first subset of mice was first treated with 5 mg/kg osimertinib QD until the emergence of resistant tumors, then switched to 25 mg/kg osimertinib QD to confirm resistance. All other mice were treated with 25 mg/kg osimertinib continuously from the start. Mice that exhibited progressive disease or stable disease on 25 mg/kg osimertinib were then either sacrificed for analysis of resistance mechanisms, or switched to 25 mg/kg erlotinib, 25 mg/kg afatinib, 7.5 mg/kg afatinib, or combination erlotinib plus osimertinib (both 25 mg/kg).

### Tumor Sequencing

Tumors were flash frozen in liquid nitrogen and ground to a powder. RNA was extracted using the RNeasy Mini Kit (Qiagen #74106), and RNA was treated with Dnase I (Qiagen #79254). cDNA was synthesized using the Superscript III First-Strand Synthesis System for RT-PCR (Invitrogen

#18080-051). Regions of interest in the *EGFR* transgene and *Kras* cDNA were amplified using the HotStarTaq Master Mix Kit (Qiagen #203443) and sequenced. *Met* amplification was assessed by quantitative PCR (*see below*).

**Primers for Tumor Sequencing**

The following primers were used for sequencing of cDNA amplified from osimertinib-resistant mouse tumors: EGFR-2074F (CTTACACCCAGTGGAGAAGC), EGFR-2502R (CACCAAGCGACGGTCCTCCA), EGFR-2445F (CAACTGGTGTGTGCAGATCG), EGFR-3616R (CACTGCTTGGTGGCGCGCGAC), mKrasF (AGAGAGGCCTGCTGAAAATG), and mKras-432R (CCCTCCCCAGTTCTCATGTA). Sub-cloning was performed using the TOPO TA Cloning Kit for Sequencing (Thermo Fisher Scientific #K457501).

**Next Generation Sequencing of Osimertinib-resistant GEMM Tumors**

cDNA from same L858R+T790M osimertinib-resistant tumors previously made (described above) was PCR-amplified using the HotStarTaq Master Mix Kit (Qiagen #203443) and the following primers: 2065F (GTGGAGCCTCTTACACCCAG), 2337R (GGTGGAGGTGAGGCAGATG), 2337F (CATCTGCCTCACCTCCACC), and 2585R (TTCTTTCTCTTCCGCACCCA). The PCR products were then library-prepped using the KAPA HyperPrep Kit (#KK8504), KAPA Dual-Indexed Adapter Kit (#KK8722), and KAPA Pure Beads (#KK8000). The samples were pooled and sequenced on a NovaSeq 6000 (Illumina) using 2 x 150 seq bp paired end reads. The analysis first aligned the reads to the amplicon sequences using the Burroughs-Wheeler aligner [3], and an in-house script was used to count each base seen in the reads for each position of the amplicon reference.

**Tumor Growth Rate Modeling**

We assume that tumor dynamics follow a branching process where one tumor cell can either give rise to two daughter cells or die [4, 5]. Additionally, we suppose that tumors are a mixture of two or more different cell types: cells that are sensitive to the treatment, and cells that have developed a resistance to the drug through a known mechanism. For the purpose of this analysis, we focused only on the proliferation and death kinetics of the cells and not on the acquisition of further mutations over time. We converted tumor volumes from mice to tumor cell count [6] in order to model cell proliferation. We assume that the resistant tumor cells dominate the tumor population once there is no observed sensitivity or tumor volume reduction (i.e. complete resistance). Thus, we used observations from each tumor after resistance or stable tumor volume under osimertinib. For each treatment group, we fit a linear mixed effect model using the NLME package in the R statistical software [7]. In all models, we regressed the natural log tumor cell count on the treatment day with effect modification due to a resistance mutation, and we incorporated a random slope to account for the dependency of observations within mice. The estimated coefficient of an effect modification represents a cell proliferation rate which is interpreted as the change of the number of tumor cells per day on the natural log scale. When assessing a statistically significant difference in proliferation rates between resistance mechanisms, we obtained p-values using two-sided t-tests of the appropriate coefficients from the regressions.

When comparing the effects of a treatment (first-line osimertinib versus second-line erlotinib or first-line osimertinib versus second-line afatinib), we performed a cross-over analysis by measuring the proliferation rates at periods of different treatment for each sequential regimen, adjusting for the resistance mechanism. This is likewise achieved by using mixed effect models.

**CRISPR design, cell transfection and drug treatment**

The two guide RNAs (crRNA) targeting exon 18 and exon 20 of EGFR (**Supplementary Table S2**) were designed using the CRISPR design tool at http://crispr.mit.edu. The different single strand donor DNAs (ssDNA) containing the mutation of interest (L718Q (T2153A); L718V

(C2152G)) or C797S+T790M coupled with a silent mutation in the PAM motif (to avoid the recognition of the edited allele by the CRISPR/Cas9 system) were purchased from IDT. The Cas9 protein was produced in house at AstraZeneca as previously described [8]. For PC9, PC9-VanR, and II-18 cells, $2 \times 10^5$ cells were electroporated using the Neon® Transfection System 10 µL Kit (Thermo Fisher Scientific). 0.27µl of 100µM of both crRNA (IDT) and tracrRNA (IDT) were added to 0.46µl of a nuclease-free duplex buffer and heated to 95°C for 5 min then left at RT. The gRNA-tracrRNA duplex was then mixed with 1uL of purified Cas9 protein (1µg/µL) to form the ribonucleoproteic complex (RNP). 5µl of Resuspension Buffer R, 1µL of a ssDNA (0.007nmol/µL) or an enhancer (**Supplementary Table S2**) were then mixed to the RNP complex and incubated at RT for 15 min. Cells were re-suspended in $2 \times 10^5$ cells/5µL Resuspension Buffer R and then mixed with Cas9 RNPs. A 10 µl sample was taken for each electroporation using the optimization program 16 (1400V, 20ms, 2 pulses). For each condition, two transfections were pooled together and seeded as follows: PC9 cells, $0.4 \times 10^5$ and $1.2 \times 10^5$ of transfected cells into two different 6 well plates containing RPMI media, 10% FCS, 1X GlutaMAX. For PC9-VanR cells, $0.33 \times 10^5$ and $2 \times 10^5$ of transfected cells were seeded into two different 6 well plates containing RPMI media, 2% FCS, 1X GlutaMAX. For II-18 cells, $6.6 \times 10^5$ of transfected cells were seeded into two 6 well plates containing RPMI media, 10% FCS, 1X GlutaMAX.

Three days after the transfection, cells from one well were collected and frozen to form the ‘pre’ samples. In parallel, the second wells were treated with osimertinib for 3-4 weeks: 100nM for PC-9 cells in RPMI, 10% FCS, 1X Glutamax for the first three days, then increased to 300nM of osimertinib; 500nM for PC9-VanR cells in RPMI, 2% FCS, 1X Glutamax; 50nM for II-18 cells in RPMI, 10% FCS, 1X Glutamax. Every 3-4 days the cell confluency was assessed using Cell Metric (Solentim). After 3-4 weeks of treatment, PC9, PC9-VanR, and II-18 cells were collected and frozen to form the ‘post’ selection samples.

**Sanger Sequencing for CRISPR experiments**

Genomic DNA was extracted from frozen pellets using DNA Blood/Tissue Kit (Qiagen). Region of interest in the *EGFR* transgene was amplified using Phusion Flash High-Fidelity PCR Master Mix (ThermoFisher #F548S) and the primers described in **Supplementary Table S2**. The PCR products were sequenced by Sanger sequencing.

**Next Generation Sequencing for CRISPR experiments**

Genomic DNA was extracted from frozen pellets using DNA Blood/Tissue Kit (Qiagen). PCR1 amplicons were generated in 20 cycles using primers containing adapter sequences as stated in **Supplementary Table S2**. Indexing primers were added in a second PCR step with a further 10 cycles using 1 ng of purified PCR product from PCR1. For all PCR reactions, amplicons were cleaned-up using MAGBIO magnetic beads and amplicon size was validated using the QIAxcel (QIAGEN). Libraries were quantified using qubit fluorometer (Qubit dsDNA HS Assay Kit, ThermoFisher Scientific) or the Fragment Analyzer using the dsDNA kit (Advanced Analytical Technologies, Ankeny, IA), pooled and sequenced on a MiSeq (Illumina) using a MiSeq Reagent Kit v3 (2 × 300 bp paired end reads) or a NextSeq 500 (Illumina) using a NextSeq 500/550 Mid Output v2 kit (2 × 150 bp paired end reads). The analysis of each sample mapped the paired reads to the target amplicon of EGFR [or Human genome (version hg19/GRCh37)] using the Burroughs-Wheeler aligner [3]. The sequence alignment map (SAM) files were processed to determine the mutation frequencies using a perl script. A second script was used to categorize the different mutation combinations for each expected codon change as to whether the change occurred alone, co-occurred with other SNPs, or with other indels, or both. These categories were further divided based on whether the other SNPs were expected silent or PAM mutations.

**Transient transfections and Western blot analysis**

Cells were plated at 2 x $10^5$ cells/well in 6 well plates in DMEM with 10% FBS. On day 2, cells were transfected with the pcDNA3.1(-) plasmid containing $EGFR^{L858R}$ (*plasmid courtesy of William*

*Pao*), with or without the additional resistance mutations C797S, L718V, L718Q (added using QuikChange II Site-Directed Mutagenesis Kit, Agilent Technologies #200523). Transfections were performed using FuGENE HD Transfection Reagent (Promega #E2311). On day 4, cells were serum starved. On day 5, cells were treated with TKI for 1 hour, then washed with PBS and lysed in cold RIPA lysis buffer (50nM Tris HCl [pH 9.0], 150 mM NaCl, 5 mM MgCl, 1% Triton X-100, 0.5% sodium deoxycholate, 0.1% SDS, and protease and phosphatase inhibitor cocktail; Thermo Scientific). Protein concentration was quantified and equal amounts of total protein were loaded, separated by SDS-PAGE, and probed as indicated. Signals were detected using SuperSignal West Pico chemiluminescent substrates (Pierce Biotechnology). List of antibodies: EGFR (CST #2232, 1:1000), pEGFR-Y1068 (CST #3777, 1:1000; CST #2234), $EGFR^{L858R}$ (CST #3197, 1:1000), $EGFR^{del746\_750}$ (CST #2085, 1:1000), $RAS^{G12V}$ (CST #14412), and β-actin (Sigma #A2066, 1:2000; CST #12620).

**Quantitative PCR**

Genomic DNA from pulverized tumors and adjacent normal lung was extracted using the DNeasy Blood & Tissue Kit (Qiagen #69505). Quantitative PCR was performed with TaqMan copy number assays (Applied Biosystems) using a ViiA7 Real Time PCR System (Applied Biosystems). Ten nanograms of genomic DNA were used in the reaction. Amplification was carried out for 40 cycles (10 minutes at 95°C, 15 seconds at 95°C, 1 minute at 60°C). Quadruplicate $C_t$ values were averaged and normalized to genomic DNA from the tail of an FVB mouse. A TaqMan copy number reference assay for mouse Tfrc (Applied Biosystems) was used for all the reactions. Met copy number was evaluated using the following primers: Mm00193012_cn and Mm00192999_cn.

**Molecular dynamics studies**

A starting model was generated using the crystal structure of the EGFR-L858R kinase domain (aa 695-988: PDB ID 2ITV) [9]. This structure was initially subjected to the ‘protein preparation

wizard' available in the Schrödinger Suite 2018-3 [10], to remove adenylyl imidodiphosphate and solvent water molecules. The missing amino acids were added and minimized using Prime. Geometry minimization of the subsequent structure was verified by gradient convergence (Polak-Ribier Conjugate Gradient with a threshold of 0.005). The resulting structure was then used as a starting point for generating subsequent models of the L718Q and L718V kinase domain mutants (in an L858R context) with- and without the relevant bound inhibitors. Full geometry optimizations on each model systems were performed using the Optimized Potentials for Liquid Simulations (OPLS3e) force field with simulated water (SGB solvation model) available under the Schrödinger Suite 2018-3 running on the Macintosh platform [10-12]. To verify convergence and consistency of the optimizations, a number of examples were re-optimized from multiple starting points; energetic variations of 0.1 kcal/mol or less were found among these calculated structures.

A conformational search (Prime) on a segment (aa. 863-876) of the flexible activation loop revealed several local minima (>20) within 3.0 kcal/mol. Given the nature of the implicit solvation model, it is not straightforward to establish the biological relevance (although important) of these conformations and their influence on the corresponding protein-inhibitor complexes. Hence, a single lowest energy conformer (rather than a Boltzman distribution) was used for comparison of the un-ligated kinase domains and their corresponding inhibitor-bound forms.

In the context of the L858R mutation, introduction of either L718V or L718Q mutation results in loss of binding energy upon formation of the protein-inhibitor complex in each case, consistent with the observation that L718 interacts directly with the inhibitor in all published crystal structures. Although the absolute numbers cannot be translated into biochemical or biological reality, the reductions in energy of drug binding to the L718V mutant compared with unmutated were 23.0 kcal/mol (osimertinib), 20.2 kcal/mol (erlotinib), and 18.8 kcal/mol (afatinib). Corresponding numbers for the L718Q mutation were 27.9 kcal/mol (osimertinib), 20.2 kcal/mol (erlotinib), and 23.3 kcal/mol (afatinib).

**Statistics**

Statistical analysis was performed with GraphPad Prism 8.0 software with the appropriate tests as indicated in the text and figure legends. For growth rate estimates, p-values were obtained by performing t-tests with the null hypothesis of no difference in growth rates between resistance mechanisms. Fisher's exact test was used to determine differences in the frequency of a particular resistance mechanism in different models or treatment groups. P values of less than 0.05 were considered significant. For patient cfDNA statistical analysis, values were not corrected for multiple comparisons as this was an exploratory study.

**Supplementary References**


1. Pirazzoli V, Ayeni D, Meador CB, Sanganahalli BG, Hyder F, de Stanchina E*, et al.* Afatinib plus Cetuximab Delays Resistance Compared to Single-Agent Erlotinib or Afatinib in Mouse Models of TKI-Naive EGFR L858R-Induced Lung Adenocarcinoma. *Clin Cancer Res*. **2016**;22(2):426-35.

2. Papademetris X, Jackowski MP, Rajeevan N, DiStasio M, Okuda H, Constable RT*, et al.* BioImage Suite: An integrated medical image analysis suite: An update. *Insight J*. **2006**;2006:209.

3. Li H, Durbin R. Fast and accurate short read alignment with Burrows-Wheeler transform. *Bioinformatics*. **2009**;25(14):1754-60.

4. Nowell PC. The clonal evolution of tumor cell populations. *Science*. **1976**;194(4260):23-8.

5. Foo J, Michor F. Evolution of acquired resistance to anti-cancer therapy. *J Theor Biol*. **2014**;355:10-20.

6. Del Monte U. Does the cell number 10(9) still really fit one gram of tumor tissue? *Cell Cycle*. **2009**;8(3):505-6.

7. Pinheiro J. NLME: Linear and Nonlinear Mixed Effects Models. **2018**.

8. Rueda FO, Bista M, Newton MD, Goeppert AU, Cuomo ME, Gordon E*, et al.* Mapping the sugar dependency for rational generation of a DNA-RNA hybrid-guided Cas9 endonuclease. *Nat Commun*. **2017**;8(1):1610.

9. Yun CH, Boggon TJ, Li Y, Woo MS, Greulich H, Meyerson M*, et al.* Structures of lung cancer-derived EGFR mutants and inhibitor complexes: mechanism of activation and insights into differential inhibitor sensitivity. *Cancer Cell*. **2007**;11(3):217-27.

10. Banks JL, Beard HS, Cao Y, Cho AE, Damm W, Farid R*, et al.* Integrated Modeling Program, Applied Chemical Theory (IMPACT). *J Comput Chem*. **2005**;26(16):1752-80.

11. Harder E, Damm W, Maple J, Wu C, Reboul M, Xiang JY*, et al.* OPLS3: A Force Field Providing Broad Coverage of Drug-like Small Molecules and Proteins. *J Chem Theory Comput*. **2016**;12(1):281-96.

12. Roos K, Wu C, Damm W, Reboul M, Stevenson JM, Lu C*, et al.* OPLS3e: Extending Force Field Coverage for Drug-Like Small Molecules. *J Chem Theory Comput*. **2019**;15(3):1863-74.

**Supplementary Table S1. Osimertinib resistance mutations occur in *cis* with L858R.**

| Tumor number | Resistance mutation | Number of L858R-positive clones | Number of clones with resistance mutation | Frequency of resistance mutations in *cis* with L858R |
|---|---|---|---|---|
| E0466 T1 | L718Q | 9/9 | 9/9 L718Q | 9/9 (100%) |
| E0465 T1 | C797S | 10/10 | 7/10 C797S<br>3/10 WT | 7/7 (100%) |
| E0377 T1 | C797S | 8/8<br>(L858R+T790M) | 4/8 C797S<br>4/8 WT | 4/4 (100%) |
| E0333 T3 | L718V | 8/8 | 8/8 L718V | 8/8 (100%) |
| E0449 T2 | L718Q | 10/10 | 10/10 L718Q | 10/10 (100%) |
| E0387 T1 | C797S | 8/8 | 8/8 C797S | 8/8 (100%) |

**Supplementary Table S2. Guide RNA, ssDNA and PCR primer sequences for NGS of CRISPR-edited cells.**

| **Guide RNA** | |
|---|---|
| **Name** | **Sequence 5'-3'** |
| Guide EGFR 18 | ATACACCGTGCCGAACGCAC |
| Guide EGFR 20 | CTGCGTGATGAGCTGCACGG |
| **ssDNA** | |
| **Name** | **Sequence 5'-3' (a)** |
| L718Q | GACTCTGGGCTCCCCACCAGACCATGAGAGGCCCTGCGGCCCAGC CCAGAGGCCTGTGCCAGGGACCTTACCTTATACACCGTGCCGAAC GCACC**t*** GAGCCC**t**GCACTTTGATCTTTTTGAATTCAGTTTCCTTCAA GATCCTCAAGAGAGCTTGGTTGGGAGCTTCTCCACTGGGTGTAAGA GGCTCCACAAGCTGGGG |
| L718V | GACTCTGGGCTCCCCACCAGACCATGAGAGGCCCTGCGGCCCAGC CCAGAGGCCTGTGCCAGGGACCTTACCTTATACACCGTGCCGAAC GCACC**t*** GAGCCCA**c**CACTTTGATCTTTTTGAATTCAGTTTCCTTCAA GATCCTCAAGAGAGCTTGGTTGGGAGCTTCTCCACTGGGTGTAAGA GGCTCCACAAGCTGGGG |
| C797S+T790M | CCAGGAAGCCTACGTGATGGCCAGCGTGGACAACCCCCACGTGTG CCGCCTGCTGGGCATCTGCCTCACCTC**a*** ACCGTGCAGCTCATCA**t**G CAGCTCATGCCCTTCGG**a**T**c**CCTCCT**c**GACTATGTCCGGGAACACAA AGACAATATTGGCTCCCAGTACCTGCTCAACTGGTGTGTGCAGATC GCAAAGGTAATCAGGG |
| enhancer | GGACGTAGCCTTCGGGCATGGCGGACTTGAAGAAGTCGTGCTGCT TCATGTGGTCGGGGTAGCGGCTGAAGCACTGCACGCCGTAGGTCA |

| | |
|---|---|
| | AAGTGGTGACGAGGGTGGGCCAGGGCACGGGCAGCTTGCCGGTGGTGCA |
| | |
| **PCR primers for EGFR exon 18 NGS** | |
| **Name** | **Sequence 5'-3' (b)** |
| EGFR Exon18 NGS Fw | TCGTCGGCAGCGTCAGATGTGTATAAGAGACAGGCTGAGGTGACCCTTGTCTC |
| EGFR Exon18 NGS Rv | GTCTCGTGGGCTCGGAGATGTGTATAAGAGACAGACAGCTTGCAAGGACTCTGG |

(a) Mutations compared to the endogenous sequence are indicated in lowercase letters.

* PAM silent mutation

(b) The adapter sequences are underlined, and are followed by the sequences complementary with EGFR (not underlined).

**Supplementary Table S3. Specific *Kras* mutations found in TKI-resistant tumors.**

| GEM Model | TKI Treatment | # of *Kras*-mutant Tumors | Specific mutation present |
|---|---|---|---|
| L858R | Osimertinib | 27 | G12D (5), G12R (2), G12V (7), G13D (1), G13R (2), Q61H (5), Q61L (1), Q61R (4) |
| L858R+T790M | Osimertinib | 7 | G12D (2), G12V (2), Q61R (3) |
| L858R | Osimertinib → erlotinib | 9 | G12D (1), G12R (1), G12V (3), Q61H (1), Q61L (1), Q61R (2) |
| L858R | Osimertinib → 25 mg/kg afatinib | 8 | G12D (1), G12V (1), G13R (2), Q61H (3), Q61R (1) |
| L858R | Osimertinib → 7.5 mg/kg afatinib | 2 | Q61H (1), Q61R (1) |
| L858R | Osimertinib → osimertinib + erlotinib | 4 | Q61H (2), Q61R (2) |
| L858R | Combination first-line osimertinib + erlotinib | 9 | G12D (1), G12R (2), G12V (3), Q61H (1), Q61R (2) |

**Supplementary Table S4. Patient biopsy information and additional genomic alterations detected in the tumor.** All three biopsies were performed on the liver. Mutant allele frequency (MAF) of *EGFR* mutations are shown, as well as all other alterations detected in other genes.

| Timepoint | Sequencing | *EGFR* Mutations (MAF %) | Other Genomic Alterations |
|---|---|---|---|
| 4/20/2018 Diagnosis | Targeted NGS Panel | L858R (84.6%) | None |
| 3/29/2019 Osimertinib Progression | Foundation One CDx | L858R (84%)<br>L718Q (73%)<br>L718V (3%) | *EGFR* amplification, *BCL2L2* amplification, *MYC* amplification, *BRD4* splice site 2212-58_2430del277, *CDKN2A/B* loss exon 2, *EPHB4* amplification, *FGF10* amplification, *MTAP* loss exons 6-8, *NFKBIA* amplification, *NKX2-1* amplification, *TP53* G245S, *AKT1* amplification, *FLT1* R812Q, *GNAS* F620L, *HRAS* P169fs*31, *MED12* Q2119_G2120insHQQQ, *MKNK1* H141L, *NBN* amplification, *PARK2* rearrangement, *PARP2* amplification, *RAD21* amplification, *RAD51B* amplification, *SPEN* D1778_A1783del, *STAG2* amplification, *ZNF217* M410V |
| 9/25/2019 Afatinib Progression | Foundation One CDx | L858R (88%)<br>L718V (80%)<br>L718Q (3%)<br>T790M (59%) | *EGFR* amplification, *BCL2L2* amplification, *BRD4* splice site 2212-58_2430del277, *CDKN2A/B* loss exon 2, *MTAP* loss exons 6-8, *NFKBIA* amplification, *NKX2-1* amplification, *TP53* G245S, *FLT1* R812Q, *GNAS* F620L, *HRAS* P169fs*31, *MED12* Q2119_G2120insHQQQ, *MKNK1* H141L, *NBN* amplification, *PARK2* rearrangement, *PARP2* amplification, *SPEN* D1778_A1783del, *ZNF217* M410V |

**Supplementary Table S5. RECIST1.1 measurements for the patient case report.** Both CT scans (3/12/19 and 6/11/19) were performed with IV contrast. Target lesion 2 corresponds to the nodule in **Figure 6B**.

| Timepoint | Target Lesion 1: Left Lower Lobe Lung Nodule | Target Lesion 2: Right Upper Lobe Lung Nodule | Target Lesion Sum |
|---|---|---|---|
| 3/12/2019 Osimertinib Progression | 10 mm | 8 mm | 18 mm |
| 6/11/2019 Afatinib Response | 9 mm | Resolved | 9 mm |

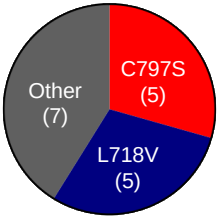


**Supplementary Figure S1. Mechanisms of resistance in tumors treated with a lower dose of osimertinib.** Pie-charts illustrating the resistance mechanisms found in osimertinib-resistant tumors, treated first with 5 mg/kg osimertinib then switched to 25 mg/kg.

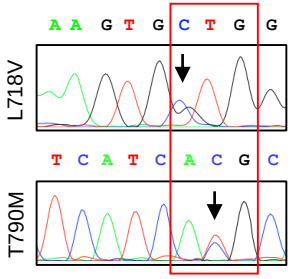


**Supplementary Figure S2. The osimertinib-resistant EGFR$^{L858R+T790M}$ GEMM tumor that gained L718V also lost T790M.** Sanger sequencing traces showing gain of L718V and loss of T790M in the same tumor.

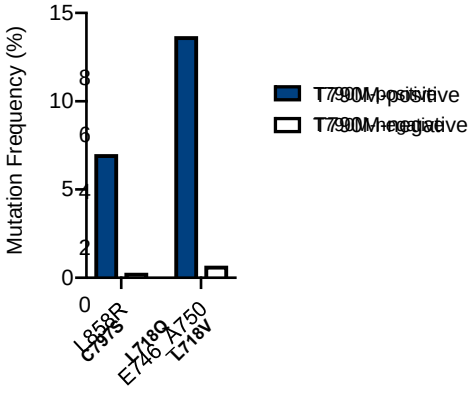


**Supplementary Figure S3. The ratio of C797S mutations is similar in T790M-positive and T790M-negative tumors in the L858R versus E746_A750 subgroups.** Graphs showing the frequency of the EGFR C797S mutation in cases with the indicated baseline *EGFR* mutation.

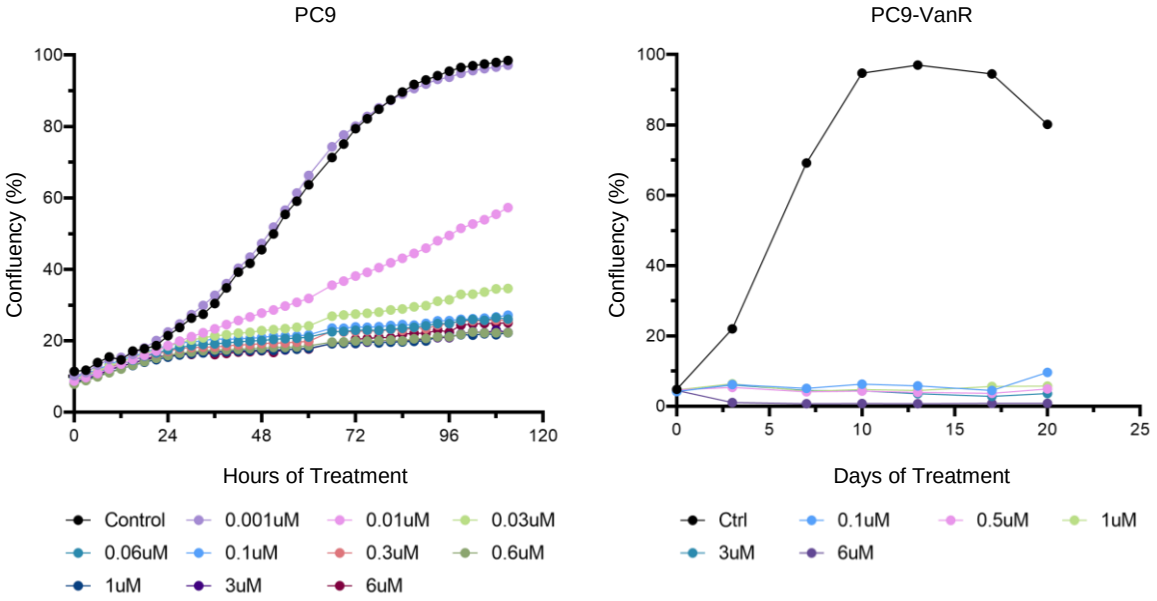


**Supplementary Figure S4. Osimertinib kill curves for PC9 (left) and PC9 –VanR (right) cells.** The concentrations are as indicated.

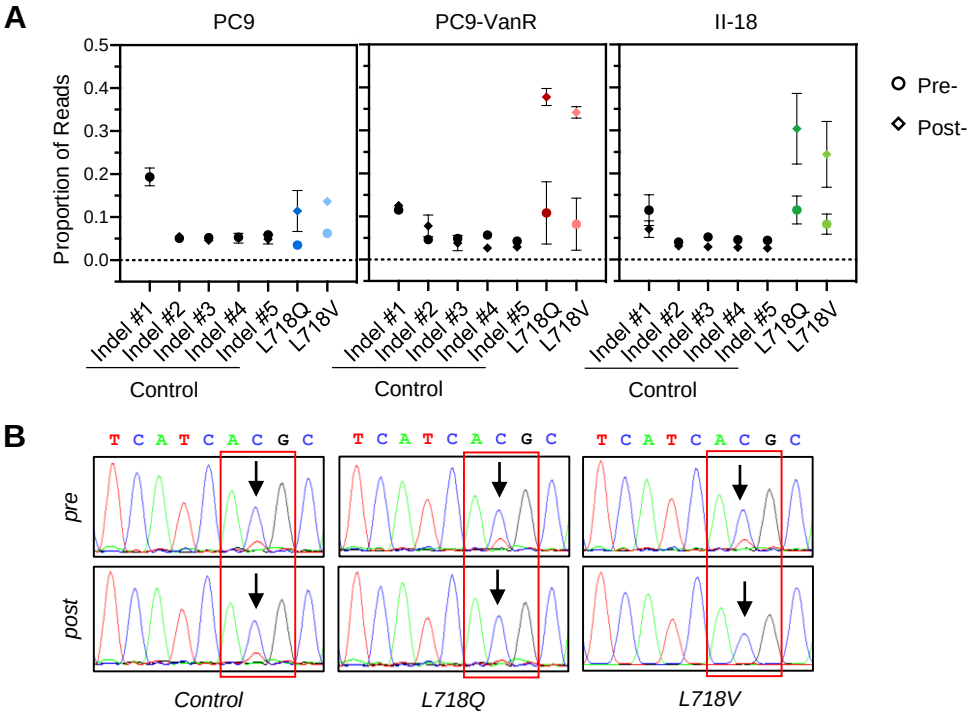


**Supplementary Figure S5. Next generation sequencing and histograms for pre- versus post- osimertinib samples. A.** Histograms show the proportion of reads for the indicated codon in the corresponding sample before osimertinib selection (pre) and the sample collected after osimertinib treatment (post). As a reference, the top 5 indels (*indel* in legend) found in the control sample are shown. The dashed line is the threshold of the background. The data for PC9 reflects the results of 3 biological replicates and PC9-VanR and II-18 reflect the results for 2 biological replicates sequenced individually. Errors bars show SEM. **B.** Sanger sequencing of the pre- and post-treatment samples of CRISPR-edited-PC9-VanR cells showing a portion of the EGFR exon 20 containing the T790 codon (red squares). The arrow shows the C→T mutation leading to T790M mutation.

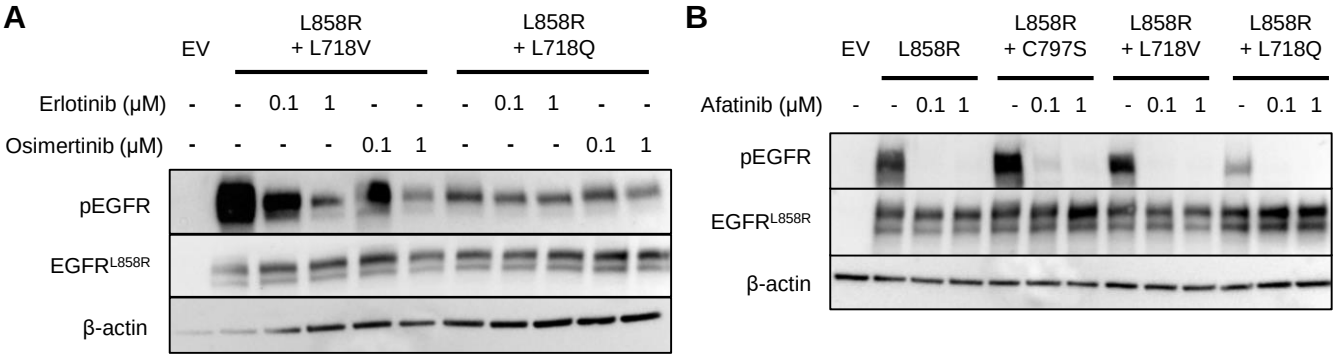


**Supplementary Figure S6. Dose-dependent changes in EGFR phosphorylation after erlotinib and afatinib treatment. A-B.** Western blots of 293T cells transiently transfected with pcDNA3.1(-) containing EGFR with the indicated mutations, treated for one hour with varying concentrations of TKI as indicated.

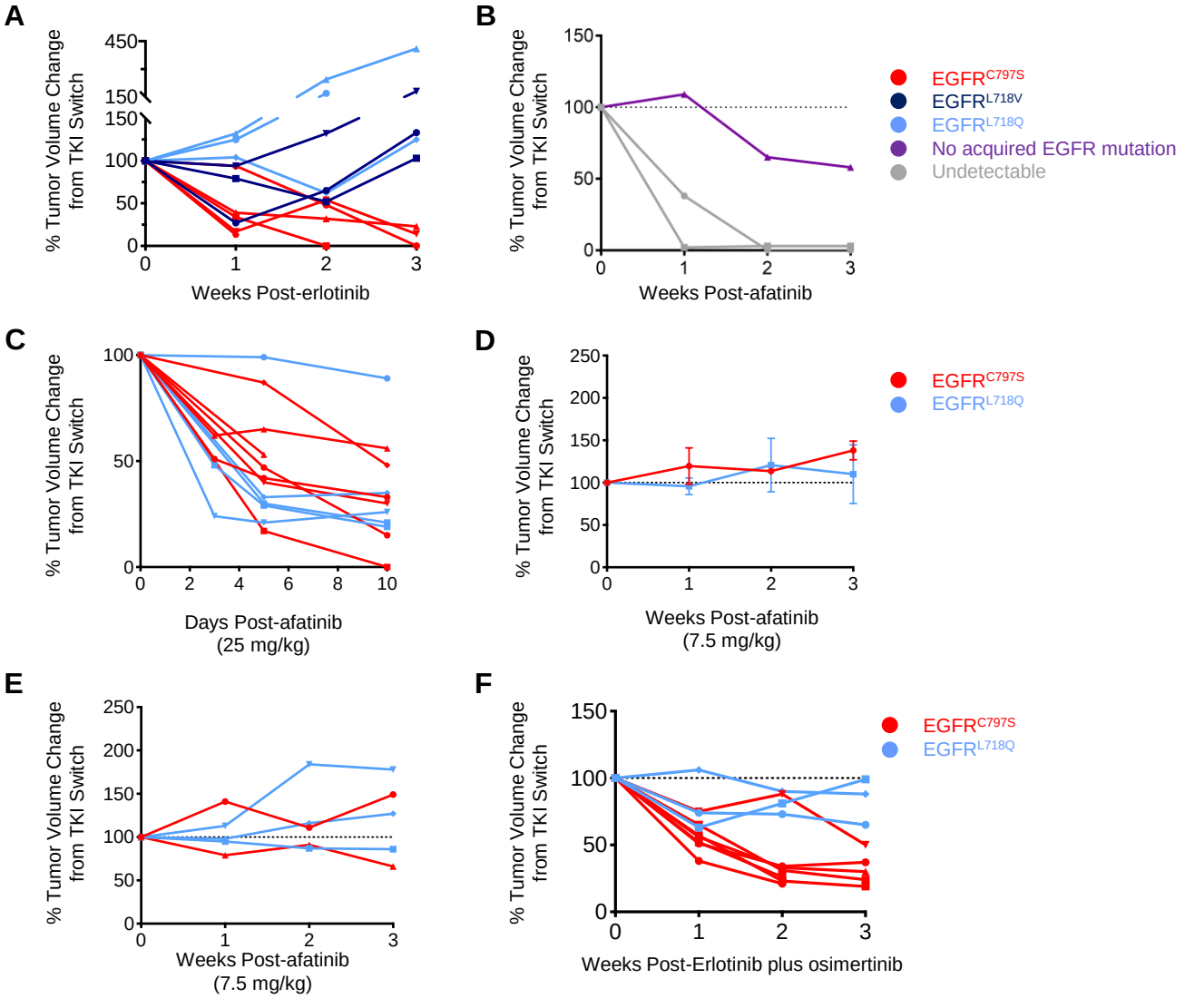


**Supplementary Figure S7. Growth curves of individual osimertinib-resistant tumor switched to erlotinib or afatinib. A, B, C, E, and F.** Tumor growth curves for the individual osimertinib-resistant tumors switched to erlotinib (**A**), 25 mg/kg afatinib (**B** and **C**), 7.5 mg/kg afatinib (**E**), or combination erlotinib plus osimertinib (25 mg/kg each; **F**) as determined by quantification of MRIs. **D.** Tumor growth curves for the average of the tumors switched to 7.5 mg/kg afatinib (n=5 total tumors; C797S n=2; L718Q n=3). **A, C, D, E** and **F** show tumors that had acquired secondary mutations in *EGFR*, while **B** shows tumors that were either not able to be sequenced or did not acquire a secondary *EGFR* mutation.

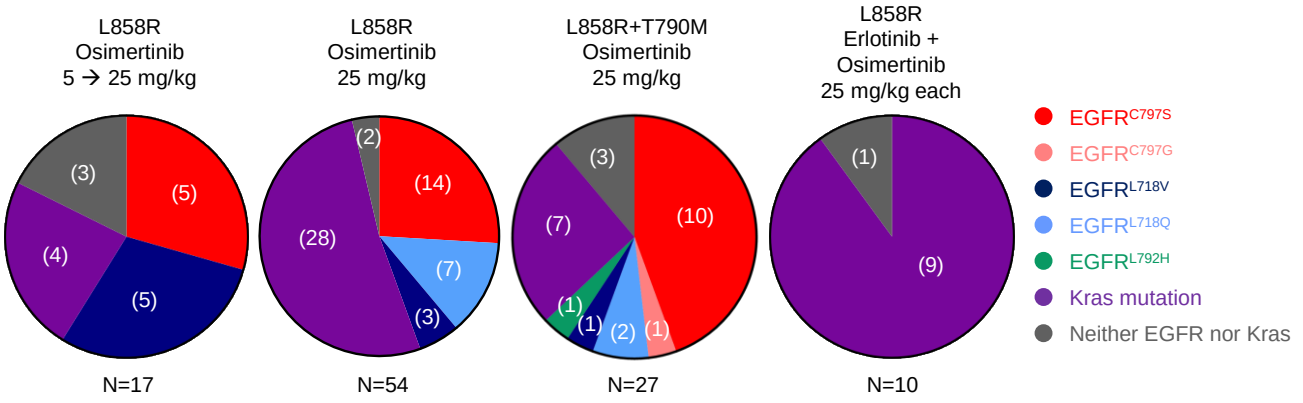


**Supplementary Figure S8. Mutations in *Kras* confer resistance to osimertinib in tumors that do not acquire secondary *EGFR* mutations.** Pie charts indicating the frequency of *Kras* mutations in osimertinib-resistant tumors in the indicated GEM models.

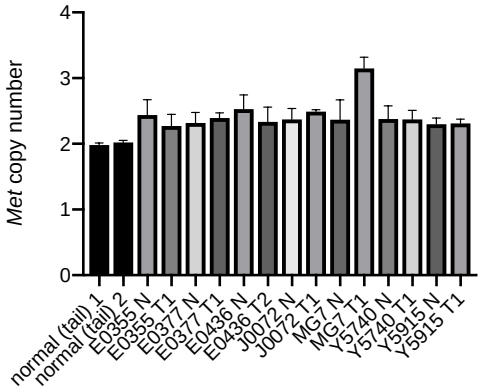


**Supplementary Figure S9. Additional molecular testing on osimertinib-resistant tumors.** *Met* copy number assay for osimertinib-resistant GEMM tumors that did not acquire an *EGFR* or *Kras* mutation. Data from experimental samples are normalized to genomic DNA from the tail of an FVB mouse. The mean of 4 technical replicates and the standard error are shown for each sample. 'N', matched adjacent normal lung; 'T', tumor.